ENVIRONMENTAL RESEARCH
LETTERS

PURPOSE-LED
PUBLISHING™

LETTER • OPEN ACCESS

Simulated sensitivity of the Amazon rainforest to extreme drought

To cite this article: Phillip Papastefanou *et al* 2024 *Environ. Res. Lett.* **19** 124072

View the article online for updates and enhancements.

You may also like

- How wildfires increase sensitivity of Amazon forests to droughts
Renan Le Roux, Fabien Wagner, Lilian Blanc et al.
- Resilience of Amazon rainfall to CO_2 removal forcing
Suqin Zhang, Xia Qu, Gang Huang et al.
- Opposite eco-hydrological processes in flood and drought years caused comparable anomaly in dry-season canopy growth over southern Amazon
Huixian Zhang and Yi Liu

This content was downloaded from IP address 141.5.20.126 on 25/11/2024 at 11:48

ENVIRONMENTAL RESEARCH
LETTERS

LETTER

Simulated sensitivity of the Amazon rainforest to extreme drought

Phillip Papastefanou[1,*], Thomas A M Pugh[2], Allan Buras[3], Katrin Fleischer[4], Thorsten E E Grams[3], Thomas Hickler[5], David Lapola[6], Daijun Liu[7], Christian S Zang[8] and Anja Rammig[3]

[1] Department Biogeochemical Signals, Max–Planck-Institute for Biogeochemistry, Hans-Knoll-Str., 10, Jena 07745, Thuringia, Germany
[2] Department of Physical Geography and Ecosystem Science, Lund University, Lund, Sweden
[3] Technical University of Munich, Professorship of Land Surface-Atmosphere Interactions, TUM School of Life Sciences, Freising, Germany
[4] Vrije Universiteit Amsterdam, Amsterdam, The Netherlands
[5] Senckenberg Biodiversity and Climate Research Centre (BiK-F), Frankfurt/Main, Germany
[6] University of Campinas—UNICAMP, Campinas, Brazil
[7] University of Vienna, Vienna, Austria
[8] University of Applied Sciences Weihenstephan-Triesdorf, Professorship of Forests and Climate Change, Freising, Germany
* Author to whom any correspondence should be addressed.

E-mail: papa@bgc-jena.mpg.de

Keywords: Amazon rainforest, drought impacts, plant hydraulics, vegetation modeling

Supplementary material for this article is available online

OPEN ACCESS

RECEIVED
25 July 2023

REVISED
25 October 2024

ACCEPTED FOR PUBLICATION
6 November 2024

PUBLISHED
22 November 2024

Original Content from this work may be used under the terms of the Creative Commons Attribution 4.0 licence.

Any further distribution of this work must maintain attribution to the author(s) and the title of the work, journal citation and DOI.

Abstract

The Amazon rainforest is highly biodiverse and has the largest extent of the remaining intact tropical forests in the world. To this day, undisturbed tropical forests act as a carbon sink by taking up about 15% of anthropogenic carbon emissions per year. However, in the past decades, a declining trend in the carbon sink capacity in the Amazon rainforest has been observed due to increased carbon losses and tree mortality. The causes are disputed, but increasing temperatures and more frequent severe droughts are potentially major drivers. We employ a novel modeling framework and hypothesize that previously rare, extreme droughts in the Amazon, such as the ones in 2005 and 2010, constitute the main cause behind the decline of the net carbon sink in aboveground biomass. Our dynamic vegetation model simulates process-based plant hydraulics and drought-induced mortality, and accounts for the diversity of strategies in plant responses to drought based on observed hydraulic vulnerability curves. The simulated impact of the 2005 drought event temporarily turned the annual Amazon net carbon sink to a carbon source of about 0.25 Mg C ha^{-1} . In contrast to other dynamic vegetation models our model simulated an increasing trend in carbon losses and a declining trend in the Amazon carbon sink over the past 25 years (net sink rate of −0.015 Mg C ha^{-1} $year^{-1}$ or −0.18 Mg C ha^{-1} per decade) which corresponds well with long-term forest monitoring data (net sink rate of −0.016 Mg C ha^{-1} $year^{-1}$). We show that this trend is entirely attributable to drought-induced forest mortality during extreme years. The simulations show a threshold-like behavior between drought intensity and biomass loss, which is due to xylem vulnerability, indicating the potentially high sensitivity of Amazon forests to extreme drought. Further increases in the severity and frequency of droughts might thus lead to greater carbon release and tree mortality than previously assumed.

1. Introduction

Over the past decades, undisturbed forests in the Amazon basin rendered a net carbon sink in its aboveground biomass (AGB), indicating greater carbon uptake by photosynthesis than carbon losses (Brienen *et al* 2015, Hubau *et al* 2020). However, observational data indicate that this sink is declining (Brienen *et al* 2015, Hubau *et al* 2020) and that the Amazon rainforest may turn into a carbon source by 2030 (Hubau *et al* 2020). Several mechanisms explaining the declining sink are being discussed,

© 2024 The Author(s). Published by IOP Publishing Ltd

for example, increased atmospheric CO_2 concentration inducing greater growth rates but also greater carbon losses (Bugmann and Bigler 2011, Quesada *et al* 2012, Hubau *et al* 2020) or increasing frequency and intensity of extreme climate events, such as droughts, leading to reduced carbon gains and increased losses (Yang *et al* 2018). Locally, extreme drought events have been observed to lower forest productivity and increase tree mortality and carbon losses, whilst regionally severe droughts such as the ones in 2005 and 2010 have turned the Amazon carbon sink into a temporary carbon source (Lewis *et al* 2011, Feldpausch *et al* 2016). However, the role of drought stress in the long-term decline of the Amazon carbon sink is still unclear.

Process-based modeling offers the possibility to mechanistically attribute cause. Earth system models exhibit significant variability in their simulations of the tropical carbon sink (Koch *et al* 2021), potentially caused by factors such as different process representations, no consensus on how the species diversity can be condensed into plant functional types (PFTs), and the challenge of simulating tropical precipitation patterns (Fiedler *et al* 2020). However, most models project a continuous increase in the tropical carbon sink in the future, mainly due to plant-physiological effects of increased atmospheric CO_2 concentrations (Huntingford *et al* 2013, Koch *et al* 2021). CO_2 fertilization on carbon gains, albeit limited by nutrient availability in some models (Fleischer *et al* 2019), outweigh negative climate impacts in future simulations (Arora *et al* 2020) and the simulations show no increasing carbon losses compared to the observations (Koch *et al* 2021). The unrealistic representation of forest drought response in process-based vegetation models may lead to this mismatch. This is exemplified by an ensemble of vegetation models that failed to reproduce drought-induced tree mortality from two throughfall exclusion experiments (TFEs) in the Central Amazon basin (Powell *et al* 2013). Recent results indicate that failure of the plant hydraulic system is directly associated with tree death in many ecosystems (Rowland *et al* 2015, Hammond *et al* 2019), however, only very few models link plant hydraulics directly to mechanisms of death in models (Fang *et al* 2022). Recent model improvements based on new theories and more detailed implementation of plant hydraulics provide avenues for simulating plant responses to drought stress (e.g. Xu *et al* 2016, Eller *et al* 2018, Kennedy *et al* 2019, De Kauwe *et al* 2020, Yao *et al* 2023).

Despite having often been associated with one of the key mechanisms leading to death under drought stress, particularly in the Amazon basin (Rowland *et al* 2015), mortality related to hydraulic failure is not considered by the standard version of LPJ-GUESS and only by very few other published dynamic global vegetation models (DGVMs) at the current time (Fang *et al* 2022, Yao *et al* 2023). Most other DGVMs only indirectly simulate mortality associated with drought stress: plant stomatal closure minimizes water loss but also carbon uptake. In turn, overall growth is reduced and models implement an empirical relationship that increases mortality when growth is reduced (e.g. (Smith *et al* 2014)). Traditional DGVMs often include only a single evergreen and a single raingreen tropical PFT, differing primarily in their leaf habit parameterization (Smith *et al* 2014). This simplification may be insufficient to capture the complexity of tropical ecosystems, especially under drought conditions. The large variety of functional strategies among tropical tree species can buffer responses to drought (Anderegg *et al* 2018). Site-level observations suggest a wide range of hydraulic strategies across Amazonian tree species, including different tolerances of the xylem to low stem water potentials (supporting figures 1 and 2, (Oliveira *et al* 2019, Bittencourt *et al* 2020)) and different strategies for maintaining or reducing transpiration under drought (Garcia *et al* 2021). The diversity of functional hydraulic strategies is expected to lead to more nuanced impacts of extreme drought.

Here, we use the dynamic vegetation model LPJ-GUESS that combines a detailed representation of vegetation dynamics and ecosystem biogeochemistry and has been widely tested (Smith *et al* 2014, Pugh *et al* 2019, Terrer *et al* 2021, Döscher *et al* 2022). We extend LPJ-GUESS by introducing a novel plant hydraulic architecture that links plant responses to drought, from reduced photosynthesis to tree mortality from hydraulic failure, termed LPJ-GUESS-HYD. We model the role of plant diversity by simulating an ensemble of 37 individual plant water-regulation strategies (PWS) based on available xylem vulnerability data (pairs of ψ_{50} and ψ_{88} from (Oliveira *et al* 2019, Bittencourt *et al* 2020)), diverse stomatal behavior in response to drought stress (Papastefanou *et al* 2020), and other hydraulic trade-offs (see supporting table 1, methods and supporting methods 6).

2. Materials and methods

2.1. LPJ-GUESS standard model description

The DGVM LPJ-GUESS simulates the exchange of water, energy, carbon and nitrogen between the land and atmosphere. The model has been applied for numerous regional (e.g. Dass *et al* 2018, Bastos *et al* 2020) and global simulation studies (e.g. Pugh *et al* 2019) and is capable of predicting functional, compositional, and structural properties of ecosystems of the major climate zones of the Earth (Smith *et al* 2014). LPJ-GUESS features individual-based vegetation dynamics (GUESS: General Ecosystem Simulator, Smith *et al* 2001) accounting for growth, mortality, and other processes of individual age cohorts of trees.

In the standard version of LPJ-GUESS (v4.0) a maximum conductance of the canopy in absence of water stress is estimated assuming full stomatal opening, based on daily CO_2, daylight, and shortwave radiation (Smith *et al* 2014). The conductance of the canopy controls the calculation of photosynthetic carbon uptake. For simulating transpiration, the model estimates a patch-specific water demand based on equilibrium evapotranspiration (Haxeltine and Prentice 1996). The patch-specific water demand needs to be supplied from water in two soil layers. If the available soil water does not meet the water demand, canopy conductance for photosynthetic carbon uptake is downregulated following an empirical hyperbolic relationship (Haxeltine and Prentice 1996, Huntingford and Monteith 1998). In the current implementation the rooting depth distribution is fixed to 60% of the fine roots in the top 50 cm of the soil and 40% between 50 cm and 150 cm of soil depth. Transpired water is then taken out of each soil layer weighted by the fraction of fineroots in each layer. Standard LPJ-GUESS includes multiple additive mortality mechanisms for trees, including, a patch destroying disturbance, a mortality mechanism associated with fire, a bioclimatic limit mortality (prescribing the low temperatures limits within a given PFT can survive), a background, longevity-based mortality (Pugh *et al* 2020), and a growth-efficiency based mortality. Only the fire-related and growth efficiency mortality can be dynamically linked to drought stress.

The standard version of LPJ-GUESS does not simulate individual plant species, but PFTs that reduce the complexity of species diversity in ecological function to a few plant types (Bonan 2002). In the tropics, three tree PFTs are simulated, which differ in their leaf physiology and their levels of shade tolerance (Smith *et al* 2014). The growth efficiency mortality of standard LPJ-GUESS increases a PFT's chance of death if the growth rate (mainly net primary productivity) is lower compared to the previous five years. Such lower growth rates can e.g. be caused by an overshadowing by other individuals or by a reduced canopy conductance due to drought stress. Productivity is usually accumulated throughout the year and growth and mortality are only once evaluated, at the end of each calendrical year. Therefore, low productivity of a tree during a drought event can be offset by higher growth during the wet season, if both happening during the same year, so that the standard version potentially underestimates the impact of interannual variation in climate from e.g. shorter drought events.

2.2. Plant hydraulic architecture implementation

LPJ-GUESS-HYD builds on standard LPJ-GUESS incorporating a plant hydraulic architecture including a new hydraulic failure based mortality mechanism. LPJ-GUESS-HYD also extends the concept of PFTs from LPJ-GUESS to plant water-regulation strategies (PWS) which diversify the existing LPJ-GUESS PFTs into a range of strategies based on additional traits related to plant hydraulics. These parameters are described in section 'Model input and parameterization'. Since fire is rare in undisturbed moist tropical forests (Andela *et al* 2019, Li *et al* 2019), we disabled it in our simulations.

The hydraulic implementation of LPJ-GUESS-HYD splits into four different compartments: (1) The soil, leaf and xylem water potential are estimated based on soil water content and a dynamic approach considering different hydraulic strategies. (2) Hydraulic resistances of roots, stem, and leaves are derived with water potentials and sapwood viscosity. (3) Following Darcy's law and the supply-demand theory a canopy conductivity g_C is derived using (1) and (2). (4) The total evapotranspiration flux E_Σ is estimated based on the Penman-Monteith equation using g_C from (3) and a simple energy-atmosphere-balance model including aerodynamic conductance and leaf temperature. Each of the four compartments will be explained in the following sections.

2.2.1. Water potential dynamics

Soil water potential ψ_s [MPa] is derived upon an empirical relation from soil water content θ and clay- and sand-fraction according to Saxton *et al* (1988). This relationship also requires a minimum soil water potential at which plants permanently wilt, which we assume to be −3.5 MPa (Hickler *et al* 2006). For each of the soil layers *i* in LPJ-GUESS a soil water potential $\psi_{s,i}$ [MPa] is estimated and subsequently weighted with a plant specific rooting depth parameter r_i [-] (Hickler *et al* 2006). The resulting ψ_s across the soil layers is estimated as:

$$\psi_s = \sum_i \psi_{s,i} \cdot r_i \tag{1}$$

Leaf water potential ψ_L [MPa] is estimated based on an empirical and dynamic approach by solving the model from Papastefanou *et al* (2020):

$$\frac{d\psi_L}{dt} = \alpha\left((1-\lambda)\psi_s - \psi_L - \Delta\psi_{ww}\right) \tag{2}$$

where λ [-] reflects the plants' water potential regulation mechanism and $\Delta\psi_{ww}$ [MPa] the difference of $\psi_s - \psi_L$ under non-stress conditions ($\psi_s \approx 0$). $\alpha\left[d^{-1}\right]$ is a rate parameter that describes the adjustment speed of ψ_L to changes in ψ_s. We use the daily version of LPJ-GUESS for which the rate parameter can be neglected and hence we set $\alpha = 1d^{-1}$ for this study. The above equation is specially designed to capture leaf water potential dynamics under drought stress. λ and $\Delta\psi_{ww}$ can both be estimated with time series consisting of predawn and midday leaf water potential (Papastefanou *et al* 2020). Xylem water

potential follows an empirical relationship based on Fisher *et al* (2006):

$$\psi_x = b \cdot (\psi_s - \psi_L) + \psi_s \quad (3)$$

where b [-] is an empirical parameter. According to the analysis of Fisher *et al* (2006), b ranges from 0 to 0.2 and is thus much closer to ψ_s under non-stressed and between 0.5 and 0.9 closer to ψ_L under drought conditions. In the current implementation, we set $b = 0.5$.

2.2.2. Hydraulic resistances and cavitation

The total hydraulic resistance of a plant is split into three compartments, leaf resistance R_L, shoot or xylem resistance R_S and root resistance R_R, all in $m^2MPa\,s\,kg^{-1}$. Each of the resistances are calculated based on the respective water potential including a specific hydraulic failure caused loss-of-conductivity. Resistance equations are adapted from (Hickler *et al* 2006) and modified, introducing next to xylem cavitation κ_S [-], also leaf and root cavitation κ_L [-] and κ_R [-], respectively. We assume that roots are equally vulnerable to hydraulic failure compared to the xylem, and leaves are approximately twice as much vulnerable as the xylem ($\psi_{50,leaf} = 0.5 \cdot \psi_{50}$, equal slope parameter, Aroca 2012). Plants do not have an active repair mechanism of xylem embolism, instead, we assume that freshly allocated sapwood is not cavitated and has no loss of conductivity, hence the loss-of-conductivity of the total sapwood reduces when fresh sapwood is allocated. Root- and leaf cavitation are assumed to be repaired instantaneously on a daily basis, whereas xylem cavitation can only be repaired during the allocation process; once at the end of each calendrical year. Sapwood resistance is calculated as in Hickler *et al* (2006):

$$R_S = \frac{h \cdot \eta_S}{k_{S,max} \cdot (1 - \kappa_S) \cdot A_S} \quad (4)$$

with $k_{S,max}$ [$m^{-1}s^{-1}MPa^{-1}kg$]: maximum sapwood conductivity, κ_S: sapwood loss of conductivity, A_S [m^2]: sapwood area, h [m]: tree height, η_S [-]: viscosity of the sap flow. Leaf resistance is estimated as:

$$R_L = \frac{1}{k_{L,max} \cdot (1 - \kappa_L) \cdot fpc} \quad (5)$$

with $k_{L,max}$ [$m^{-1}s^{-1}MPa^{-1}kg$]: maximum leaf conductivity, fpc [-]: foliage projective cover, κ_L [-]: leaf loss of conductivity. Root resistance is calculated as:

$$R_R = \frac{\eta_R}{k_{R,max} \cdot (1 - \kappa_R)} \quad (6)$$

with $k_{R,max}$ [$s^{-1}MPa^{-1}$]: maximum root conductivity, κ_R [-]: root loss of conductivity, η_R the viscosity of the root sap. Each loss of conductivity κ of each of the three compartments ($\kappa_S, \kappa_L, \kappa_R$) is calculated according to a polynomial response curve (Santiago *et al* 2018):

$$\kappa(\psi) : \frac{1}{1 + \left(\frac{\psi}{\psi_{50}}\right)^d} \quad (7)$$

with ψ_{50} (MPa): water potential at which 50% of the compartments (leaves, roots, stem) conductivity is lost and d[-]: a slope parameter, both defined on a species or PWS level. We assume that κ_S, κ_L and κ_R depend on ψ_x, ψ_L and ψ_R, respectively. We parameterize each slope d on ψ_{50} and ψ_{88}:

$$d = -\frac{\log(0.88)}{\log\left(\frac{\psi_{88}}{\psi_{50}}\right)} \quad (8)$$

2.2.3. Hydraulic failure based mortality

We introduce a new tree mortality probability m_k related to hydraulic failure based on the loss-of-conductivity of the stem κ_S. The relation between m_k and κ_S is modeled using a Weibull relation reparametrized from Hammond *et al* (2019):

$$m_k(\kappa_S) = 1 - \exp\left(-\left(\frac{\kappa_S}{f_\kappa}\right)^{d_\kappa}\right) \quad (9)$$

with $f_\kappa = 0.85$ and $d_\kappa = 8.0$, both dimensionless. This relationship shows mortalities close to zero for values of κ_S lower then 50% loss of conductivity, but then rapidly rises to mortality probabilities over 50% once 80% of conductivity is lost. While this relationship was derived from gymnosperms, it is in agreement with other empirical studies showing that roughly 88% loss of conductivity is lethal for wide range of angiosperms (Barigah *et al* 2013, Urli *et al* 2013). Hence, we decided to use this parameterization of f_κ and d_κ for each of our PWS. Furthermore, we also include parameters f_κ and d_κ in our sensitivity study (supporting figure 3).

2.2.4. Canopy conductance

Canopy conductance g_C is calculated via Darcy's law assuming that water flow J [$kgs^{-1}m^{-2}$] from soil via roots, shoot and leaves to the atmosphere balances the imposed transpiration flux E_{imp} [$kgs^{-1}m^{-2}$] (Jarvis and McNaughton 1986, Martínez Vilalta *et al* 2014, McDowell *et al* 2016). The water flow J is estimated according to Whitehead (1998):

$$J = \frac{\Delta\psi}{R_{Total}} = \frac{\psi_s - \psi_L - \rho \cdot g \cdot h}{R_L + R_S + R_R} \quad (10)$$

and the imposed transpiration flux E_{imp} on foliage projective cover basis:

$$E_{imp} = g_C \cdot VPD. \quad (11)$$

Assuming $J = E_{imp}$ we can solve for g_C [kgs^{-1}m^{-2}kPa^{-1}]:

$$g_C = \frac{J}{\mathrm{VPD}}. \quad (12)$$

To avoid the overestimation of g_C under non-drought conditions we estimate the non-stressed canopy conductance $\widetilde{g_C}$ based on the non-stressed photosynthesis (assuming stomates fully opened) and estimate the final canopy conductivity as $\max(g_C, \widetilde{g_C})$, Following our approach, we only consider VPD affecting g_C assuming $g_C \sim \frac{1}{\mathrm{VPD}}$, hence neglecting the effect of VPD on leaf water potential ψ_L.

2.2.5. Evapotranspiration

To estimate the total evapotranspiration E_Σ [kgs^{-1}m^{-2}] we need to consider both imposed- and equilibrium evapotranspiration fluxes, E_{imp} and E_{eql} using the instructive form of the Penman-Monteith-equation (Köstner *et al* 1992):

$$E_\Sigma = E_{eql} \cdot \Omega + E_{imp} \cdot (1 - \Omega)) \quad (13)$$

where Ω [-] is a dimensionless factor that describes the coupling between the canopy and the atmosphere. Ω can be estimated as Köstner *et al* (1992):

$$\Omega = \frac{1 + \epsilon}{1 + \epsilon + \frac{g_A}{g_C}} \quad (14)$$

with ϵ [-]: change of latent heat relative to the change in sensible heat of saturated air, g_A (m s^{-1}): aerodynamic conductance. The equilibrium evapotranspiration E_{eql} is an already established part of LPJ-GUESS (Whitehead *et al* 1984, Colin Prentice *et al* 1993, Smith *et al* 2001) used to calculate the water demand of the plant in the standard model. Aerodynamic conductance g_A depends on multiple factors including wind speed and leaf temperature. It can be included into a DGVM using a coupling to an atmospheric model. We adapt the approach of Leuning (1995) to estimate g_A. Total evapotranspiration E_Σ, aerodynamic conductance g_A and leaf temperature T_L [K] form a circular dependency which we solve by recursively iterating over E_Σ, T_L and g_A starting with an initial $g_A = 40$ mm s^{-1} following (Arneth *et al* 2007).

2.2.6. Model input and parameterization

We applied our model to the Amazon Basin as delineated by the Amazon river drainage (based on (Döll and Lehner 2002), figure 1 at 0.5°× 0.5° gridded resolution. In this study, we use GLDAS 2.0 (Rodell *et al* 2004) as climate forcing dataset as it provides all necessary forcing variables for LPJ-GUESS-HYD: Precipitation, near-surface temperature, shortwave radiation, vapour pressure deficit (derived with specific humidity and atmospheric pressure, or from relative humidity) and wind speed. To account for potential bias of the forcing dataset, we reran our model using an additional forcing dataset WATCH_WFDEI (Weedon *et al* 2011) which covers a similar time span.

In the simulations, we introduce 37 hydraulic plant water regulating strategies (PWS) based on the tropical broad-leaved evergreen PFT, TrBE (Hickler *et al* 2006, Smith *et al* 2014). A PWS extends a PFT by six additional parameters that describe: the hydraulic water potential regulation (parameters λ and $\Delta\psi_{ww}$, see section 2.2.1), the maximum hydraulic conductivities of roots, stem and leaves, and stem hydraulic vulnerability curves defined by the water potentials of 50% and 88% loss of conductance, ψ_{50} and ψ_{88}, respectively. Hydraulic vulnerability curves were selected as pairs of ψ_{50} and ψ_{88} from observations from two experimental sites and other literature sources on tropical vegetation (Barros *et al* 2019, Oliveira *et al* 2019, Bittencourt *et al* 2020; supporting methods 6).

We analyzed correlations of plant traits at the species level using values from the TRY-Database (Kattge *et al* 2020) and extended sources (supporting methods 6). These data showed that ψ_{50} is positively correlated with two other parameters: SLA (specific leaf area) and k_S (stem hydraulic conductivity) (supporting figure 4). Phenomenologically, these empirical relationships can be motivated with plants that invest into a more robust xylem (lower ψ_{50}) trade this robustness off into less well conducting tissues (lower k_S), however, do also leave their stomates open for longer under drought stress (lower λ). In contrast, plants that are more vulnerable to drought stress (higher ψ_{50}) have less robust tissues that can conduct water better (higher k_S), but therefore have to close stomates earlier under drought stress (higher λ). Higher specific leaf area means that more carbon per leaf needs to be invested which could be attributed to more robust leaves that are necessary to maintain water transport with the more drought resistant xylem tissues (lower ψ_{50}).

We used these empirical relationships between ψ_{50} and k_S, and ψ_{50} and SLA to interpolate k_S and SLA based on ψ_{50} for each of our 37 PWS (supporting table 1). Based on the range of hydraulic strategies from Papastefanou *et al* (2020) we selected the entire gradient between isohydrodynamic and isohydric parametrizations as that best reproduces the field observations on water potential dynamics across different functional types and biomes (supporting table 1). Each of the 37 hydraulic PWS was run in isolation, without direct competition from other tree strategies, but including C3- and C4-grasses based on standard LPJ-GUESS parametrization (Smith *et al* 2014). All 37 PWS were simulated in each grid cell across the Amazon basin.

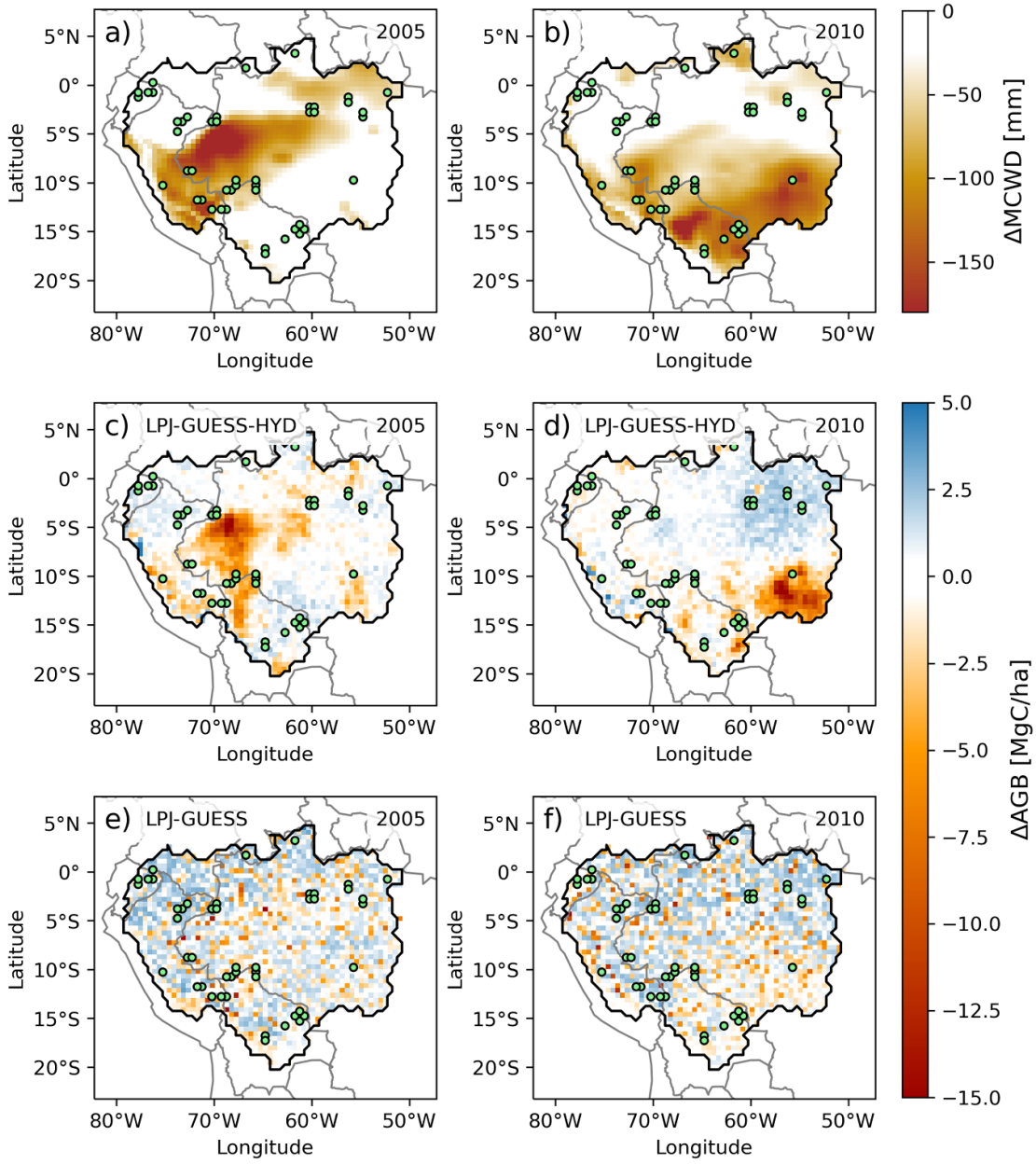

Figure 1. Spatial patterns of drought stress and impacts of 2005 and 2010 on the Amazon basin. Climatological drought stress is estimated as the maximum cumulative water deficit (MCWD) for 2005 (a) and 2010 (b). Impacts of the two drought events on simulated woody aboveground biomass (AGB) when using LPJ-GUESS-HYD (c), (d) and standard LPJ-GUESS (e), (f). The impact is calculated as median change in AGB over all PWS from 2004 to 2005 and 2009 to 2010, respectively. The green dots are the locations of the inventory plots from Brienen *et al* (2015).

2.3. Modeling protocol

Both the standard version of LPJ-GUESS and the new hydraulics version (LPJ-GUESS-HYD) have been applied independently to the 1946 grid cells representing the Amazon basin using the two forcing datasets GLDAS 2.0 (main analysis) and WATCH_WFDEI (supporting analysis). We applied 1500 years of vegetation spinup where we randomly recycle the climate forcing of the first 30 years from the input dataset. We further set a disturbance interval, that is, one over the probability that the vegetation of a forest patch in model is completely erased, to be 1000 years (Pugh *et al* 2020). With standard LPJ-GUESS we used the three tropical PFT-parameterizations of Smith *et al* (2014). With LPJ-GUESS-HYD we used the PWS parametrizations introduced in this study. For the standard LPJ-GUESS, all three PFTs competed against each other for light and nitrogen, consistent with previous studies (Smith *et al* 2014). Both model versions were also conducted with nitrogen cycling enabled. CO_2 forcing was set to dynamic which means that the CO_2 concentration of the simulation steadily increased according to the measured average annual concentrations and was set to 278 ppm during the spinup before the year 1765.

2.4. AGB anomaly calculation

LPJ-GUESS does not differentiate between above- and belowground woody biomass. Therefore, we use an empirical relationship to distribute modeled vegetation carbon into belowground biomass (BGB) and AGB (Saatchi *et al* 2011):

$$\mathrm{BGB} = 0.489 \cdot \mathrm{AGB}^{0.89} \quad (15)$$

with AGB and BGB both in Mg dry mass ha^{-1}. We used a factor of 0.5 to convert from dry mass ha^{-1} to carbon dry mass ha^{-1}. The AGB anomaly of each year was then calculated as the change from the mean AGB over the baseline period from 1984 to 2010. We further applied this relationship to estimate the amount of sapwood that is invested into above and belowground, and to partition carbon losses between above and belowground carbon.

2.5. MCWD anomaly calculation and drought classification

As a drought indicator, we applied the maximum cumulative water deficit MCWD based on Aragão *et al* (2007). We computed this drought index similarly to Lewis *et al* (2011) by accumulating the difference between monthly precipitation and evapotranspiration (ET). MCWD was calculated for the hydrological year (from October of the previous year to September of the succeeding year) for accumulating water deficit. For deriving the MCWD anomaly for 2005 and 2010 we calculated the mean MCWD for the 'baseline' period from 1984 to 2010 and subtracted the baseline period from the values of 2005 and 2010, respectively. For the calculation of MCWD we set value $\mathrm{ET}_{\mathrm{fixed}} = 100$ mm month^{-1} (Aragão *et al* 2007), which enables comparison to the empirical study of Phillips *et al* (2009) used in figure 2. Similar to Lewis *et al* (2011) we defined an MCWD anomaly $\leqslant -25$ mm as moderate drought stress because at this level, tree mortality already significantly increased in the inventory plots. We further defined an MCWD anomaly of $\leqslant -120$ mm as severe and an MCWD anomaly $\leqslant -200$ mm as extreme drought stress.

2.6. Statistical analysis

We apply simple linear regression analysis to estimate the trends of carbon gains, carbon losses and, and net carbon balance, i.e. carbon sink or carbon source for each of the simulations of the 37 PWS. We average across the 37 PWS by weighting the contribution of each PWS to, for example, overall carbon and water fluxes, by its AGB. When comparing the relationship between the anomalies of MCWD and AGB we fit a three parameter exponential model:

$$\mathrm{AGBanomaly} = -\exp\left(a \cdot \mathrm{MCWDanomaly} + b\right) + c \quad (16)$$

against the modeled (MCWD, AGB) anomaly points.

2.7. External data sources

The relationship between AGB anomaly and MCWD anomaly was digitized from figure 2(A) from Phillips *et al* (2009). TRENDY version 10 model output was obtained from the Global Carbon Budget (Friedlingstein *et al* 2022). We converted the TRENDY output variable *cVeg* to AGB and AGB anomaly following the procedure of section 2.4. Observational trends in carbon losses, gains and net sink were obtained from the source data of Hubau *et al* (2020). We evaluate our modeled AGB against estimates from inventories from Avitabile *et al* (2016). We also compare modeled AGB against basin-wide estimates based on vegetation optical depth (VOD) using the ABC dataset (Liu *et al* 2015). Furthermore, we also compare modeled anomalies in AGB with anomalies in VOD using the VODCA dataset (Moesinger *et al* 2020). Data sources used to derive our 37 PWS are described in the supporting methods 6.

3. Results and discussion

3.1. Impact of the 2005 and 2010 extreme drought events

The drought epicentre in 2005 was located in the central-western part of the Amazon basin, which was characterized by a particularly large maximum cumulative water deficit (MCWD) (figure 1(a), Phillips *et al* 2009, Papastefanou *et al* 2021). LPJ-GUESS-HYD simulations reproduced the observed AGB loss but not the standard version of LPJ-GUESS (figures 1(c) vs. (e)) despite higher overall biomass of the standard version prior to the drought event (supporting figure 5). Similarly, to standard LPJ-GUESS most state-of-the-art dynamic vegetation models do not show spatial patterns associated with drought stress (e.g. DGVMs in the TRENDY (Friedlingstein *et al* 2022) ensemble, see supporting figure 6). Simulating the drought of 2005 using LPJ-GUESS-HYD indicated an average carbon loss of 0.29 $\mathrm{MgC\,ha^{-1}yr^{-1}}$ for the 37 PWS (Quartiles: [−0.99, 0.01], figure 1(c)). Simulated carbon gains of LPJ-GUESS-HYD are similar during the 2005 drought year compared to 2004 and 2006 and feature plausible values according to long-term inventory plots (Phillips *et al* 2009). Carbon losses are higher in 2005 (mean 2.9 $\mathrm{MgC\,ha^{-1}yr^{-1}}$ (Quartiles: [2.4, 3.5]; 2004 and 2006: 2.4 $\mathrm{MgC\,ha^{-1}yr^{-1}}$)). Empirical studies generally support the strong impact of the drought in 2005 on the net carbon sink, but they disagree on whether the drought turned the Amazon basin from a sink into a source (Phillips *et al* 2009, Feldpausch *et al* 2016). According to our novel modeling approach, mortality related to low-growth and mortality related to tree age contribute about 30% and 40%, respectively, while hydraulic-failure induced mortality accounts for about 30% of the total carbon losses overall (supporting figure 7). This is in qualitative agreement

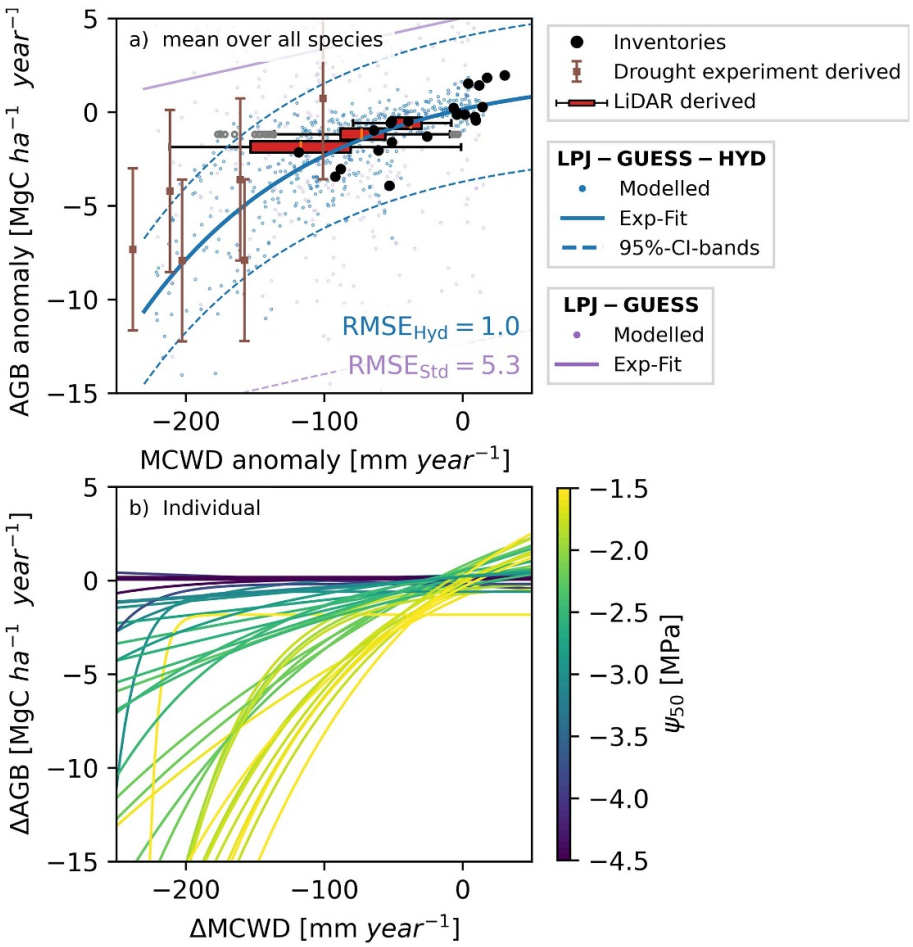

Figure 2. Relationship between drought (MCWD anomaly) and changes in simulated aboveground biomass (AGB anomaly) during the 2005 drought. (a) Blue points are the modeled responses of AGB to drought stress using the new hydraulics framework (LPJ-GUESS-HYD) with different drought intensities in 1946 grid cells covering the whole Amazon basin and averaged over the 37 plant water-regulation strategies (PWS). Black points are observational data from Phillips *et al* (2009). Brown error bars are estimates based on the Caxiuana drought experiment: AGB anomalies are derived from and MCWD anomalies from the precipitation data from Powell *et al* (2013) (see also Methods S3). Red boxplots are derived from LiDAR estimates from Yang *et al* (2018) (see also Methods S4). The blue solid line shows an exponential model fitted through the modeled points and blue dashed lines are the 0.95 confidence bands. Purple lines and points are similar to blue points using standard LPJ-GUESS instead. The confidence bands of standard LPJ-GUESS lie outside of the area plotted and are therefore only partly visible (see supporting figure 20 for the full range). (b) Individual plant water strategies (PWS) shown by the solid colored lines. Each line represents the exponential model ($y = -\exp(a \cdot x + b) + c$)) fitted to the individual PWS. The color gradient indicates the ψ_{50} of each individual PWS.

with empirical studies that emphasize the greater role of hydraulic-failure-induced mortality in tropical forests under drought stress instead of carbon starvation (Rowland *et al* 2015).

Similarly for the 2010 drought, studies based on inventory plots disagree whether the Amazon basin was a net carbon sink or source (Lewis *et al* 2011, Feldpausch *et al* 2016, Hubau *et al* 2020). LPJ-GUESS-HYD simulates a weak carbon source in 2010 across the Amazon basin (figure 1(d)) and in the subset of gridcells corresponding to the inventory plots (supporting figures 8(a) and (b)). The weaker impact of the 2010 drought in the south-eastern Amazon basin compared to the 2005 drought in central Amazonia in the model is due to more drought-resistant PWS dominating these drier areas (figures 1(b) and (d)). Furthermore, while the extreme drought events in the Amazon rainforest are often linked with the recurring sea surface temperature anomalies in the Atlantic ocean, the spatial and temporal manifestation of the drought events (e.g. 2005 and 2010) can be quite different (Lewis *et al* 2011, Marengo *et al* 2011). This, so far, has made quantifying drought stress (e.g. when expressed as MCWD anomaly) and its impact on AGB difficult to detect in observational studies and a consistent relationship between MCWD and AGB has not been found across different drought events (Feldpausch *et al* 2016). Our modeling study using the LPJ-GUESS-HYD versions, however, found consistent relationships between different drought indicators and AGB anomalies across different drought years,

albeit these were somewhat weaker in non-drought years (supporting figure 9). Similar to (Feldpausch *et al* 2016) we find a weak relationship between negative AGB anomalies and MCWD anomaly in 2010 (supporting figure 9(d)) and with VOD anomaly (supporting figure 10).

Levels of drought stress (MCWD anomaly) in the year 2005 featured a strong non-linear relationship with simulated net change in AGB (anomaly, figure 2) that matches with observed relationships derived from long-term forest inventory data (Phillips *et al* 2009), LiDAR based drought impacts (Yang *et al* 2018) and extreme drought stress based from rainfall exclusion experiments (Nepstad *et al* 2007, Rowland *et al* 2015) (figure 2(a)). LPJ-GUESS-HYD also supports the observed relationship when evaluating at the forest inventory sites of (Phillips *et al* 2009) (supporting figure 11). The version of LPJ-GUESS without plant hydraulics showed no relationship between the AGB anomaly and MCWD anomaly, inconsistent with observations from (Phillips *et al* 2009) (figure 2(a)).

While the relation between the AGB and MCWD anomalies in the inventory data is limited to 'severe' drought stress (i.e. when the MCWD anomaly is equal or less negative than -120 mm, (Phillips *et al* 2009)), our dynamic modeling approach allows assessment of extreme drought stress (e.g. MCWD anomaly ≤ -200 mm). AGB responses to such extreme drought stress have only been measured in two tropical rainfall exclusion experiments (Nepstad *et al* 2007, Rowland *et al* 2015) and our model generates similar dynamics compared to the observed biomass losses (supporting figure 12). Under such extreme drought stress, the non-linear relation between the AGB anomaly and the MCWD anomaly becomes apparent and the AGB anomaly increases roughly three-fold from MCWD anomalies of -120 mm to -200 mm (figure 2(a)). This property of the hydraulic model is in agreement with the disproportionate rise in tree mortality under extreme drought stress observed in empirical studies (Meir *et al* 2015, Rowland *et al* 2015, Arend *et al* 2021). The model thus points to a threshold-like behavior of Amazon vegetation productivity under extreme drought, which are anticipated to become more intense and more frequent under climate change (Hirota *et al* 2011).

The hydraulic strategy adopted by a tree is fundamental in its response to drought. Key aspects of the hydraulic strategy are the resistance of the xylem to embolism, the efficiency of the xylem in transporting water and whether stomatal regulation tends towards riskier (anisohydric) or conservative (isohydric) strategies (Tardieu and Simonneau 1998, Hartmann *et al* 2021). Our 37 PWS encompassed a range of strategies assuming a direct trade-off between ψ_{50} and isohydricity (less negative ψ_{50}, more isohydric), between ψ_{50} and leaf mass area (less negative ψ_{50}, higher leaf mass area) and between ψ_{50} and maximum stem conductivity $k_{s,max}$ (less negative ψ_{50}, higher $k_{s,max}$, supporting figure 4). We find a strong non-linear relationship between drought stress and impacts on AGB for a wide range of PWS (figure 2(b)). The strength of this relationship gradually declines for PWS with lower ψ_{50} (figure 2, which is consistent with empirical studies indicating species with higher xylem vulnerability to embolism display higher drought-induced mortality rates (Rowland *et al* 2015). The strongest response to the MCWD anomaly is found for PWS with $-2.2\text{MPa} < \psi_{50} < -1.4$ MPa which matches with the observations of species affected in TFEs (Rowland *et al* 2015) indicating that this particular hydraulic trait renders great risk under drought. For PWS with ψ_{50} below -3.5 MPa, we find no relationship between the MCWD and AGB anomalies, hence, such PWS may be able to withstand extreme droughts. This implies that extreme droughts impact species differently and may lead to differential resilience which is in line with physiological theory (Klein 2014).

Empirical studies found that species in the central Amazon rainforest respond rather conservatively to drought stress (closing stomates early under drought stress, isohydric behavior, higher parameter λ, (Konings and Gentine 2017, Garcia *et al* 2021)). We find a similar pattern in our modeled results with a greater dominance of more conservative PWS (higher hydraulics safety margins, supporting figure 13) in the central Amazon. However, this more conservative stomatal regulation does not prevent severe drought damage (figure 2(b)) due to the trade-off between isohydricity and xylem vulnerability. Even with closed stomates, the xylem of a plant is still at risk as water continues to escape through the closed stomates (Duursma *et al* 2019), cuticles and extremely dry soil, which can withdraw water from the plant's roots and xylem.

While we find and apply a weak empirical relationship between ψ_{50} and maximum stem conductivity $k_{S,max}$ for our PWS parameterization, other empirical studies do not support this relationship (Barros *et al* 2019, Bittencourt *et al* 2020) and the general existence of it is debated (Lens *et al* 2022). However, $k_{S,max}$ only had a minimal influence on the simulated drought response, as PWS with high $k_{S,max}$ were more vulnerable to cavitation which caused a more rapid decline of k_S under drought. Changes in $k_{S,max}$ had an impact on standing AGB under non-drought conditions, as higher $k_{S,max}$ facilitated more rapid growth. Other studies find that more dens stems are more robust against drought stress, which indicate that wood density and ψ_{50} can be correlated (Guillemot *et al* 2022). However, we could not find a significant relationship between wood density and ψ_{50} in the data sources we analyzed (supporting methods 6).

The Amazon is hyperdiverse taxonomically and very little is known about how traits and trade-offs related to drought-resistance strategies function across the region. Our results emphasize that this information is central to capturing the state and dynamics of the Amazon forest.

3.2. Long-term trends of the Amazon rainforest carbon sink

We compare net carbon balance, carbon gains, and carbon losses by their trend, magnitude, and year-to-year variability with observational data from Brienen *et al* (2015), Hubau *et al* (2020). Using a weighted mean (see section 2.6) across the PWS we find a net carbon sink over the period 1985–2010 with a mean magnitude of 0.2 MgC ha^{-1}yr^{-1} (0.2/0.8 quantiles: 0.02–0.37 MgC ha^{-1}yr^{-1}) which is lower compared to the inventories from Hubau *et al* (2020) (0.41 MgC ha^{-1}yr^{-1}, CI: 0.16–0.63 MgC ha^{-1}yr^{-1}). One of the reasons for the discrepancy between our simulations and the plot measurements may be that precipitation data in the climate forcing datasets (Papastefanou *et al* 2021) only resolve larger-scale and less local climate in the Amazon basin (supporting figure 14) and that the overall carbon storage in the Amazon basin remains quite uncertain (Tejada *et al* 2019). We find a declining trend of the net sink of −0.015 MgC ha^{-1}yr^{-2} (CI −0.002; −0.035) which is caused by a positive trend in plant carbon losses across the Amazon basin (figure 3(a), blue bold line). While carbon gains are only slightly increasing during that period (figure 3(b), slope = 0.004 MgC ha^{-1}yr^{-2}) compared to a stronger trend in the observations, carbon losses show a strong increase similar to the observations over time (figure 3(c), slope = 0.010 MgC ha^{-1}yr^{-2}). Our modeled trends are robust when applying the model to the subset of selective gridcells corresponding to the observational data (supporting figure 15 or when using a different forcing climate dataset (supporting figure 8). However, the impacts of specific years e.g. 2009 can be different (supporting figure 8). The main discrepancy in carbon gains between model and observations could be caused by our model not being able to correctly reproduce observed forest structure with the 37 PFTs, the lack of direct competition and coexistence of the PFTs for light and water, and the absence of other relevant nutrient cycling e.g. phosphorus (Fleischer *et al* 2019). Furthermore, the much lower number of plot measurements available before 1994 could also induce a bias in carbon gain observations or in the forcing dataset variables leading to a bias in modeled carbon gains.

We subdivided the modeled trend of carbon losses into the three mortality mechanisms considered in LPJ-GUESS-HYD which are related to tree age, low growth and hydraulic failure (figures 4(a)–(c), see also methods). This subdivision revealed that increasing carbon losses are largely explained by drought-induced hydraulic failure. Over 85% (32 of 37) of the simulated PWS show increasing trends in carbon losses greater than 0.01 MgC ha^{-1}yr^{-2} (average MgC 0.021 ha^{-1}yr^{-2}). Very sensitive PWS with very high $\psi_{50} > -1.2$ MPa displayed only very limited biomass growth in our model and subsequently did not show any trends (figure 4(c)).

The higher magnitude of modeled carbon losses compared to the observations might arise from the new additional mortality mechanism that we introduced and the lack of other processes important processes such as ground water uptake and hydraulic redistribution. The interplay of hydraulic failure induced mortality and the growth efficiency mortality should be further investigated as both mechanisms can co-occur. Finally, our mechanistic hydraulic failure based mortality only provides a starting point to simulate drought induced tree mortality and additional work is needed that for example conducts similar drought stress experiments as Hammond *et al* (2019) for tropical species and mature trees.

The simulation trends are in good agreement with plot inventories (Hubau *et al* 2020), but in contrast to other modeled results from (1) the Coupled Model Intercomparison Project (CMIP6, (Koch *et al* 2021)), (2) standard LPJ-GUESS (figure 3, purple line), (3) the DGVMs used in the current TRENDY ensemble (supporting figure 16), which all have not incorporated plant hydraulic failure with associated tree mortality. In these models, carbon losses are formulated as a function of carbon gains, which cannot explain the observed trends (Koch *et al* 2021). The inclusion of an mechanistic hydraulic-failure based drought mortality mechanism in LPJ-GUESS-HYD effectively decouples fluxes of carbon gain and loss (figure 3).

Similar to the impacts we found for the 2005 drought event (figure 2), the strength of the increasing trend in modeled carbon losses is related to ψ_{50} with drought-sensitive species showing a stronger increasing trend (figure 4(c)). Excluding the years with the strongest MCWD anomalies (2005, 2007, 2009, and 2010) in the GLDAS dataset from the trend calculation (figure 4(d)), we find that the increasing modeled trend in simulated drought-related mortality disappears (mean trend overall PWS: 0.001 0.021 MgC ha^{-1}yr^{-2} quartiles: 0, 0.002; figure 4(d). When excluding the recent four decades, and hence, also the recent extreme events from the climate forcing we also do not find a decreasing trend in the net carbon sink, but instead a slight increasing trend due to the CO_2 fertilization effect AGB gains (supporting figure 15). This finding highlights the Amazon rainforest's susceptibility to climate extremes such as strong El Niño events, and not to moderate drought stress per se. We generally find a higher year-to-year variability in the modeled net carbon sink of 0.49 MgC ha^{-1}yr^{-1} compared to

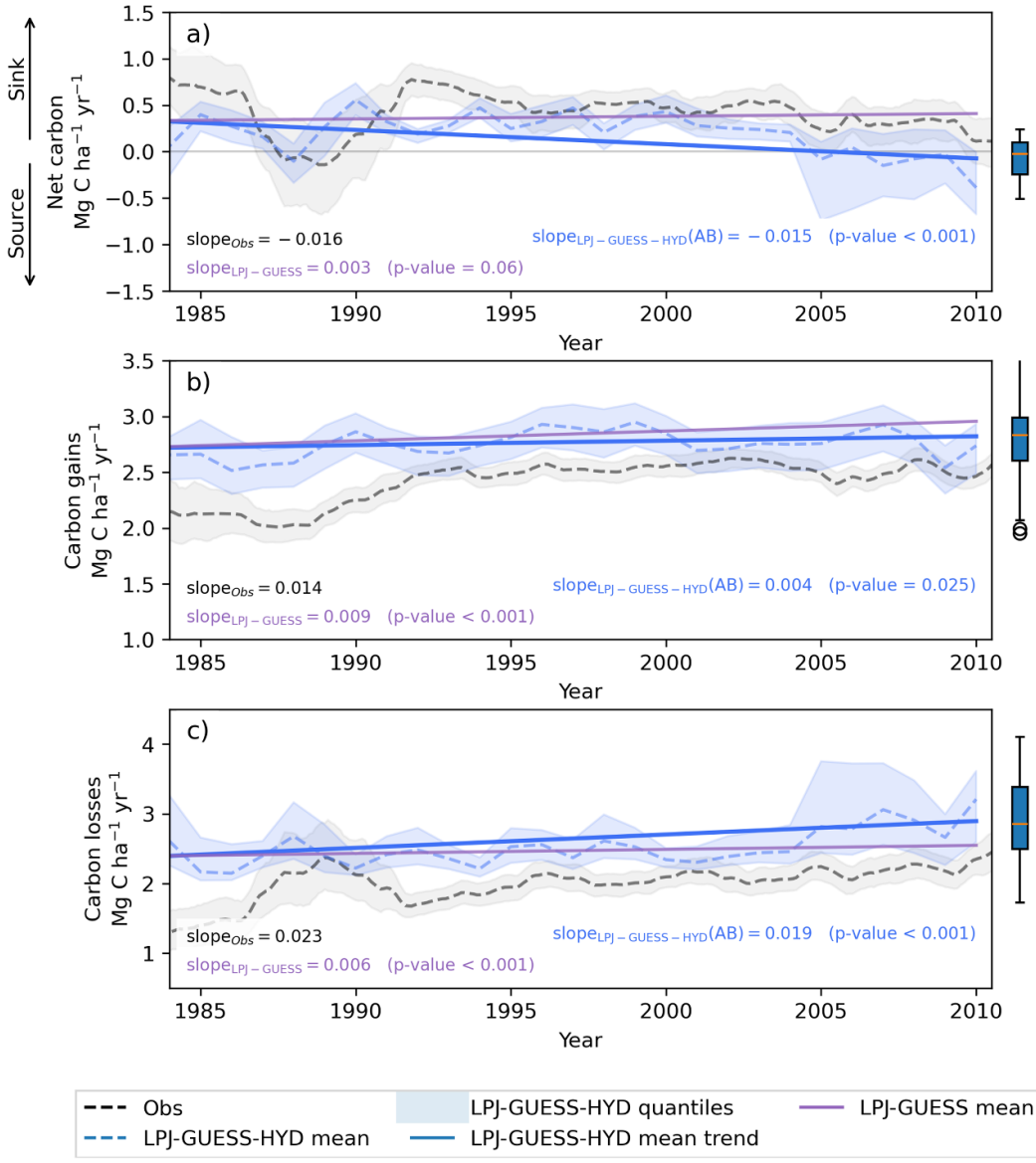

Figure 3. Yearly modeled net carbon sink rate (a), carbon gains (b) and carbon losses (c). The blue dashed line and blue area represent the two-year rolling weighted average by the AGB of each PWS, and the 0.2/0.8-quantiles over all 37 PWS and across the complete Amazon basin (AB), respectively. The solid blue line represents the trend lines of the modeled fluxes across the AB. The boxplot represents the distribution of net carbon, gains and losses in 2010 across the 37 hydraulic strategies. The purple solid line represents the trend when using standard LPJ-GUESS with default settings across the AB. As only one instance of standard LPJ-GUESS was applied no confidence bands for standard LPJ-GUESS have been calculated. The black dashed line and grey area show measurements from Brienen *et al* (2015) and Hubau *et al* (2020) (see also supporting methods S3).

observations, which is caused by a higher variability in carbon losses (0.44 MgC ha^{-1}yr^{-1}) compared to the variability in carbon gains (0.15 MgC ha^{-1}yr^{-1}). The model might thus overestimate instantaneous drought effects, however, it does not account for lag effects, which can weaken trees and increase their susceptibility to several mortality agents over several years following a drought (Peterken and Mountford 1996, Park Williams *et al* 2013, Trugman *et al* 2018, Aleixo *et al* 2019). Lag effects may cause carbon losses to extend over years, or cause compound effects, which is not considered in our model yet.

To date, only few studies have reported a clear relationship between drought stress (MCWD anomaly) and carbon losses for 2005 in the Amazon rainforest (Phillips *et al* 2009, Yang *et al* 2018). Droughts manifest in different ways across the Amazon rainforest induced by e.g. large-scale weather anomalies (Marengo *et al* 2011). There was a weaker relationship between the MCWD anomaly and biomass mortality in 2010, despite increased carbon losses (supporting figure 9(d)). Similarly, higher biomass carbon losses and lower biomass carbon gains were observed in 2010, but only the lower carbon gains could be attributed to drought stress as defined in terms of MCWD anomaly (Feldpausch *et al* 2016). Plot observations also found no relationship between MCWD and carbon losses across a network in the long-term (Hubau *et al* 2020). We find a much weaker relationship between increasing

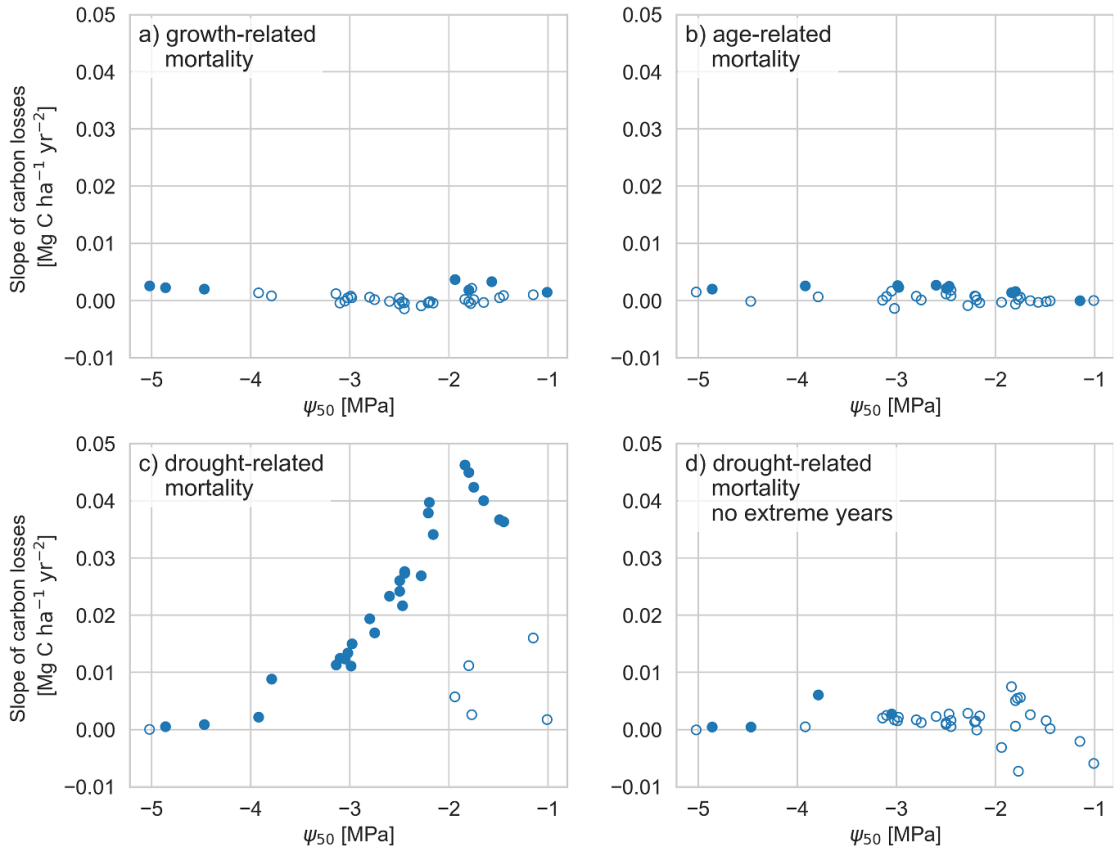

Figure 4. Scatterplots showing the individual trends (slopes) of the different mechanistic mortalities for each of 37 PWS simulated with LPJ-GUESS-HYD versus ψ_{50}, a PWS-specific parameter. The slope is based on a linear model from 1984 to 2010 for the three carbon fluxes contributing to overall mortality: (a) growth-efficiency mortality, (b) age-related mortality, (c) drought-related mortality based on hydraulic failure, and (d) similar to (c) but excluding 2005, 2007, 2009, 2010. Full circles represent slopes of a linear model with a pvalue < 0.05 and open circles with a pvalue > 0.1.

carbon losses and increasing drought stress (MCWD and MCWD anomaly) from 1984 to 2010 compared to the extreme drought event in 2005 (supporting figure 17). The strength of the relationship strongly depends on the choice of drought indicator which highlights the difficulty of measuring drought stress per se (supporting figures 9 and 17).

Multiple hypotheses have been put forward for the increasing trend in aboveground carbon losses in the Amazon rainforest (Brienen *et al* 2015, Hubau *et al* 2020). From our novel modeling approach, we conclude that hydraulic failure is the most convincing process to explain increasing carbon losses, since it is well supported by observations (Rowland *et al* 2015, Adams *et al* 2017) and—if implemented in a process-based model reproduced three lines of observational evidence; (1) modeled hydraulic failure reproduces the AGB impact of large scale drought events (figure 2); (2) improved simulated dynamics of carbon fluxes caused by artificial extreme drought stress as observed in two experimental drought experiments (Caxiuana and Tapajos, supporting figure 12), and (3) agreement with recent observed increase in carbon losses across the Amazon basin (figure 3). While our modeling study does not provide a definitive answer, we provide arguments against some of those: (1) Self thinning and growth efficiency related mortality are implemented in the standard LPJ-GUESS model and fail to capture the observed drought impacts for 2005 and the decline in net sink. (2) While a shift in species composition has been observed, it is too small to explain the observed trend in increased carbon losses (Esquivel-Muelbert *et al* 2019). (3) Accelerated growth from elevated CO_2 could also lead to increased mortality (Brienen *et al* 2020), which could explain the observed trend but not the impact of recent drought events such as 2005 and 2010 (Phillips *et al* 2009, Lewis *et al* 2011). However, we cannot rule out the increased liana abundance as a potential driver of tree mortality (Phillips *et al* 2002, Schnitzer and Bongers 2011), which should be addressed in future modeling studies. Increasing sub-lethal changes in the canopy structure of Amazon rainforests have also been observed during strong drought events (Leitold *et al* 2018) which are not considered in our model.

Our results are robust against changes of several important hydraulic parameters (supporting figures 18 and 19), while the model is very sensitive to the susceptibility of the xylem to hydraulic

failure expressed as ψ_{50} and to the mortality—loss of conductivity parametrization (supporting figure 3). Better knowledge on ψ_{50} variations and further species specific knowledge about the critical thresholds between loss-of-conductivity and mortality across the Amazon basin is important to enhance model precision. However, the extreme drought stress in rainfall exclusion experiments, which is particularly induced by soil moisture stress, is captured well by our model (figure 2(a) and supporting figure 12). Dynamic rooting depth and distribution are expected to modify the simulated effects of drought stress at the ecosystem level. While in the current implementation root distribution and depth are fixed future studies should incorporate flexible roots schemes (Sakschewski *et al* 2021) to better account for plants adaptation to environmental or drought conditions. Multiple studies also support a mortality—wood density relationship (Phillips *et al* 2019, Liang *et al* 2021), which is not yet fully understood from a mechanistic perspective and thereby not part of mechanistic mortality modeling. Both LPJ-GUESS and LPJ-GUESS-HYD are typically applied with daily forcing usually averaging or taking the maximum across sub daily timesteps. This aggregation of daily data might underestimate the effects of drought stress. For example, short and intense heat waves result in rapid changes in humidity and other environmental drivers which can influence the hydrodynamical states of plant on very short time scales.

The diversity of tropical tree species in CMIP6 models is often only represented in single PFT parameterizations (Koch *et al* 2021) which is unlikely to capture the correct response of plants under drought stress, given the diverse response of the implemented PWS in our study (figures 2(b) and 3). Weighting these PWS according to their AGB allows us to show that different PWS prevail in different climatic conditions in the Amazon (supporting figure 13). In order to simulate competition and coexistence of the PWS their plant hydraulic strategies need to be further linked to other strategies of resource partitioning and use (Oliveira *et al* 2021).

Absolute carbon loss of drought impacts does strongly dependent on biomass. Spatial patterns of biomass remain uncertain across the Amazon basin (Mitchard *et al* 2013, Tejada *et al* 2019) and both model versions LPJ-GUESS and LPJ-GUESS-HYD also differ. Here, additional studies are needed that reduce this uncertainty in biomass, e.g. utilizing VOD. Modern VOD based estimates also show a declining trend in biomass (Fan *et al* 2019) and resilience (Boulton *et al* 2022) across the Amazon basin. Better constraining the response of tropical forests to drought will also require thorough observational surveys to provide information on functional biogeography, in combination with physiological information for the different drought response types and drought-induced mortality patterns.

4. Conclusions and outlook

Plot networks have shown that the Amazon basin is turning from a net carbon sink into a carbon source much quicker than predicted by any of the state-of-the art vegetation models (Hubau *et al* 2020). One cause for this decline is presumed to be drought stress, but it has not been possible to definitively attribute this from observations. When introducing plant hydraulics to a DGVM, we showed that observed trends in tree mortality and the saturation in the Amazon carbon sink can be reproduced based on underlying ecophysiological mechanisms. The novel model approach allowed to providing attribution to drought as the primary agent of carbon balance change in these forests. This paves the way for more reliable projections of the future of tropical forests. Furthermore, we show that the rate of biomass loss is likely to accelerate following its non-linear relationship with drought intensity, at least if some of the drier climate scenarios for the region (Duffy *et al* 2015) become true. As the likelihood of extreme drought events increases in future (Trenberth *et al* 2014, Fischer *et al* 2021), our results point towards a continued, and potentially accelerating, decline of the Amazon carbon sink.

Data availability statement

The output files are about 100GB which exceeds the upper storage limits on most file hosters. The data that support the findings of this study are available upon reasonable request from the authors.

Model output is available upon request. Output scripts are available at https://github.com/PhillipPapastefanou/AmazonModellingStudy. A scatterplot of AGB anomaly vs. MCWD anomaly is available in figure 2(A) from Phillips *et al* (2009). TRENDY data sources (Friedlingstein *et al* 2022) were available after contacting Stephen Sitch and Pierre Friedlingstein. Observational trends in carbon losses, gains and net sink were obtained from the source data of Hubau *et al* (2020). Inventories of AGB were obtained from the supporting information of Avitabile *et al* (2016). The ABC dataset (Liu *et al* 2015) was accessed via www.wenfo.org/wald/global-biomass. The VODCA (Moesinger *et al* 2020) dataset can be accessed via https://doi.org/10.5281/zenodo.2575599.

Acknowledgment

We thank Rafael S Oliveira for his valuable comments and for sharing an initial dataset containing hydraulic traits of species in the Amazon rainforest. We thank the TRENDY coordinators Stephen Sitch and Pierre Friedlingstein and the TRENDY modellers for sharing model output.

Code availability

LPJ-GUESS development is managed and the code maintained in a permanent repository at Lund University, Sweden. Source code is normally made available on request to research users. Conditions apply in the case of model versions still under active development. The model version presented in this paper is identified by the permanent revision number r9954 in the code repository. There is no DOI associated with the code.

ORCID iDs

Phillip Papastefanou https://orcid.org/0000-0002-4613-2565
Allan Buras https://orcid.org/0000-0003-2179-0681
Daijun Liu https://orcid.org/0000-0002-0993-0832

References

Adams H D *et al* 2017 A multi-species synthesis of physiological mechanisms in drought-induced tree mortality *Nat. Ecol. Evol.* **1** 1285–91
Aleixo I, Norris D, Hemerik L, Barbosa A, Prata E, Costa F and Poorter L 2019 Amazonian rainforest tree mortality driven by climate and functional traits *Nat. Clim. Change* **9** 384–8
Andela N, Morton D C, Giglio L, Paugam R, Chen Y, Hantson S, van der Werf G R and Randerson J T 2019 The global fire atlas of individual fire size, duration, speed and direction *Earth Syst. Sci. Data* **11** 529–52
Anderegg W R L *et al* 2018 Hydraulic diversity of forests regulates ecosystem resilience during drought *Nature* **561** 538–41
Aragão L E O C, Malhi Y, Roman-Cuesta R M, Saatchi S, Anderson L O and Shimabukuro Y E 2007 Spatial patterns and fire response of recent Amazonian droughts *Geophys. Res. Lett.* **34** L07701
Arend M, Link R M, Patthey R, Hoch G, Schuldt B and Kahmen A 2021 Rapid hydraulic collapse as cause of drought-induced mortality in conifers *Proc. Natl Acad. Sci.* **118** e2025251118
Arneth A *et al* 2007 Process-based estimates of terrestrial ecosystem isoprene emissions: incorporating the effects of a direct CO_2-isoprene interaction *Atmos. Chem. Phys.* **7** 31–53
Aroca R 2012 *Plant Responses to Drought Stress, Plant Responses to Drought Stress: From Morphological to Molecular Features* (Springer) p 466
Arora V K *et al* 2020 Carbon-concentration and carbon-climate feedbacks in CMIP6 models and their comparison to CMIP5 models *Biogeosciences* **17** 4173–222
Avitabile V *et al* 2016 An integrated pan-tropical biomass map using multiple reference datasets *Glob. Change Biol.* **22** 1406–20
Barigah T S, Charrier O, Douris M, Bonhomme M, Herbette S, Améglio T, Fichot R, Brignolas F and Cochard H 2013 Water stress-induced xylem hydraulic failure is a causal factor of tree mortality in beech and poplar *Ann. Bot.* **112** 1431–7
Barros F d V *et al* 2019 Hydraulic traits explain differential responses of Amazonian forests to the 2015 El Niño-induced drought *New Phytol.* **223** 1253–66
Bastos A *et al* 2020 Direct and seasonal legacy effects of the 2018 heat wave and drought on European ecosystem productivity *Sci. Adv.* **6** eaba2724
Bittencourt P R L *et al* 2020 Amazonia trees have limited capacity to acclimate plant hydraulic properties in response to long-term drought *Glob. Change Biol.* **26** 3569–84
Bonan G B 2002 *Ecological Climatology: Concepts and Applications* (Cambridge University Press)
Boulton C A, Lenton T M and Boers N 2022 Pronounced loss of Amazon rainforest resilience since the early 2000s *Nat. Clim. Change* **12** 271–8
Brienen R J W *et al* 2020 Forest carbon sink neutralized by pervasive growth-lifespan trade-offs *Nat. Commun.* **11** 4241
Brienen R J W *et al* 2015 Long-term decline of the Amazon carbon sink *Nature* **519** 344–8
Bugmann H and Bigler C 2011 Will the CO2 fertilization effect in forests be offset by reduced tree longevity? *Oecologia* **165** 533–44
Colin Prentice I, Sykes M T and Cramer W 1993 A simulation model for the transient effects of climate change on forest landscapes *Ecol. Modelling* **65** 51–70
Dass P, Houlton B Z, Wang Y and Warlind D 2018 Grasslands may be more reliable carbon sinks than forests in California *Environ. Res. Lett.* **13** 074027
De Kauwe M G *et al* 2020 Identifying areas at risk of drought induced tree mortality across South-Eastern Australia *Glob. Change Biol.* **26** 5716–33
Duffy P B, Brando P, Asner G P and Field C B 2015 Projections of future meteorological drought and wet periods in the Amazon *Proc. Natl Acad. Sci.* **112** 13172–7
Duursma R A, Blackman C J, Lopéz R, Martin-StPaul N K, Cochard H and Medlyn B E 2019 On the minimum leaf conductance: its role in models of plant water use and ecological and environmental controls *New Phytol.* **221** 693–705
Döll P and Lehner B 2002 Validation of a new global 30-min drainage direction map *J. Hydrol.* **258** 214–31
Döscher R *et al* 2022 The EC-Earth3 Earth system model for the coupled model intercomparison project 6 *Geosci. Model Dev.* **15** 2973–3020
Eller C B *et al* 2018 Modelling tropical forest responses to drought and El Niño with a stomatal optimization model based on xylem hydraulics *Phil. Trans. R. Soc.* B **373** 20170315
Esquivel-Muelbert A *et al* 2019 Compositional response of Amazon forests to climate change *Glob. Change Biol.* **25** 39–56
Fan L *et al* 2019 Satellite-observed pantropical carbon dynamics *Nat. Plants* **5** 944–51
Fang Y, Leung L R, Knox R, Koven C and Bond-Lamberty B 2022 Impact of the numerical solution approach of a plant hydrodynamic model (v0.1) on vegetation dynamics *Geosci. Model Dev.* **15** 6385–98
Feldpausch T R *et al* 2016 Amazon forest response to repeated droughts *Glob. Biogeochem. Cycles* **30** 964–82
Fiedler S *et al* 2020 Simulated tropical precipitation assessed across three major phases of the coupled model intercomparison project (CMIP) *Mon. Weather Rev.* **148** 3653–80
Fischer E M, Sippel S and Knutti R 2021 Increasing probability of record-shattering climate extremes *Nat. Clim. Change* **11** 689–95
Fisher R A, Williams M, Do Vale R L, Da Costa A L and Meir P 2006 Evidence from Amazonian forests is consistent with isohydric control of leaf water potential *Plant Cell Environ.* **29** 151–65
Fleischer K *et al* 2019 Amazon forest response to CO_2 fertilization dependent on plant phosphorus acquisition *Nat. Geosci.* **12** 736–41
Friedlingstein P *et al* 2022 Global carbon budget 2021 *Earth Syst. Sci. Data* **14** 1917–2005
Garcia M N, Ferreira M J, Ivanov V, dos Santos V A H F, Ceron J V, Guedes A V, Saleska S R and Oliveira R S 2021 Importance of hydraulic strategy trade-offs in structuring response of canopy trees to extreme drought in central Amazon *Oecologia* **197** 13–24
Guillemot J *et al* 2022 Small and slow is safe: on the drought tolerance of tropical tree species *Glob. Change Biol.* **28** 2622–38
Hammond W M, Yu K, Wilson L A, Will R E, Anderegg W R L and Adams H D 2019 Dead or dying? Quantifying the point

of no return from hydraulic failure in drought induced tree mortality *New Phytol.* **223** 1834–43
Hartmann H, Link R M and Schuldt B 2021 A whole-plant perspective of isohydry: stem-level support for leaf-level plant water regulation *Tree Physiol.* **41** 901–5
Haxeltine A and Prentice I 1996 BIOME3: an equilibrium terrestrial biosphere model based on ecophysiological constraints, resource availability and competition among plant functional types *Glob. Biogeochem. Cycles* **10** 693–709
Hickler T, Prentice I C, Smith B, Sykes M T and Zaehle S 2006 Implementing plant hydraulic architecture within the LPJ dynamic global vegetation model *Glob. Ecol. Biogeogr.* **0** 060811081017001
Hirota M, Holmgren M, Van Nes E H and Scheffer M 2011 Global resilience of tropical forest and savanna to critical transitions *Science* **334** 232–5
Hubau W *et al* 2020 Asynchronous carbon sink saturation in African and Amazonian tropical forests *Nature* **579** 80–87
Huntingford C and Monteith J L 1998 The behaviour of a mixed-layer model of the convective boundary layer coupled to a big leaf model of surface energy partitioning *Bound.-Layer Meteorol.* **88** 87–101
Huntingford C *et al* 2013 Simulated resilience of tropical rainforests to CO_2-induced climate change *Nat. Geosci.* **6** 268–73
Jarvis P and McNaughton K 1986 Stomatal control of transpiration: scaling up from leaf to region *Adv. Ecol. Res.* **15** 1–49
Kattge J *et al* 2020 TRY plant trait database - enhanced coverage and open access *Glob. Change Biol.* **26** 119–88
Kennedy D, Swenson S, Oleson K W, Lawrence D M, Fisher R, Lola da Costa A C and Gentine P 2019 Implementing plant hydraulics in the community land model, version 5 *J. Adv. Modeling Earth Syst.* **11** 485–513
Klein T 2014 The variability of stomatal sensitivity to leaf water potential across tree species indicates a continuum between isohydric and anisohydric behaviours *Funct. Ecol.* **28** 1313–20
Koch A, Hubau W and Lewis S L 2021 Earth system models are not capturing present day tropical forest carbon dynamics *Earth's Future* **9** e2020EF001874
Konings A G and Gentine P 2017 Global variations in ecosystem scale isohydricity *Glob. Change Biol.* **23** 891–905
Köstner B M M *et al* 1992 Transpiration and canopy conductance in a pristine broad-leaved forest of Nothofagus: an analysis of xylem sap flow and eddy correlation measurements *Oecologia* **91** 350–9
Leitold V, Morton D C, Longo M, dos-Santos M N, Keller M and Scaranello M 2018 El Niño drought increased canopy turnover in Amazon forests *New Phytol.* **219** 959–71
Lens F, Gleason S M, Bortolami G, Brodersen C, Delzon S and Jansen S 2022 Functional xylem characteristics associated with drought-induced embolism in angiosperms *New Phytol.* **236** 2019–36
Leuning R 1995 A critical appraisal of a combined stomatal-photosynthesis model for C3 plants *Plant Cell Environ.* **18** 339–55
Lewis S L, Brando P M, Phillips O L, van der Heijden G M F and Nepstad D 2011 The 2010 Amazon Drought *Science* **331** 554–554
Li F *et al* 2019 Historical (1700-2012) global multi-model estimates of the fire emissions from the Fire Modeling Intercomparison Project (FireMIP) *Atmos. Chem. Phys.* **19** 12545–67
Liang X, Ye Q, Liu H and Brodribb T J 2021 Wood density predicts mortality threshold for diverse trees *New Phytol.* **229** 3053–7
Liu Y Y, van Dijk A I J M, de Jeu R A M, Canadell J G, McCabe M F, Evans J P and Wang G 2015 Recent reversal in loss of global terrestrial biomass *Nat. Clim. Change* **5** 470–4
Marengo J A, Tomasella J, Alves L M, Soares W R and Rodriguez D A 2011 The drought of 2010 in the context of historical droughts in the Amazon region: drought Amazon 2010 *Geophys. Res. Lett.* **38** n/a–n/a
Martínez Vilalta J, Poyatos R, Aguadé D, Retana J and Mencuccini M 2014 A new look at water transport regulation in plants *New Phytol.* **204** 105–15
McDowell N G *et al* 2016 Multi-scale predictions of massive conifer mortality due to chronic temperature rise *Nat. Clim. Change* **6** 295–300
Meir P, Wood T E, Galbraith D R, Brando P M, Da Costa A C L, Rowland L and Ferreira L V 2015 Threshold responses to soil moisture deficit by trees and soil in tropical rain forests: insights from field experiments *BioScience* **65** 882–92
Mitchard E T, Saatchi S S, Baccini A, Asner G P, Goetz S J, Harris N L and Brown S 2013 Uncertainty in the spatial distribution of tropical forest biomass: a comparison of pan-tropical maps *Carbon Balance Manage.* **8** 10–10
Moesinger L, Dorigo W, de Jeu R, van der Schalie R, Scanlon T, Teubner I and Forkel M 2020 The global long-term microwave vegetation optical depth climate archive (VODCA) *Earth Syst. Sci. Data* **12** 177–96
Nepstad D C, Tohver I M, Ray D, Moutinho P and Cardinot G 2007 Mortality of large trees and lianas following experimental drought in an amazon forest *Ecology* **88** 2259–69
Oliveira R S *et al* 2019 Embolism resistance drives the distribution of Amazonian rainforest tree species along hydro topographic gradients *New Phytol.* **221** 1457–65
Oliveira R S, Eller C B, Barros F d V, Hirota M, Brum M and Bittencourt P 2021 Linking plant hydraulics and the fast-slow continuum to understand resilience to drought in tropical ecosystems *New Phytol.* **230** 904–23
Papastefanou P, Zang C S, Angelov Z, Anderson de Castro A, Jimenez J C, Rezende L, Ruscica R, Sakschewski B, von Randow C and Rammig A 2021 Quantifying the spatial extent and intensity of recent extreme drought events in the Amazon rainforest and their impacts on the carbon cycle *Biogeosciences* **19** 3843–61
Papastefanou P, Zang C S, Pugh T A M, Liu D, Grams T E E, Hickler T and Rammig A 2020 A dynamic model for strategies and dynamics of plant water-potential regulation under drought conditions *Front. Plant Sci.* **11** 373
Park Williams A *et al* 2013 Temperature as a potent driver of regional forest drought stress and tree mortality *Nat. Clim. Change* **3** 292–7
Peterken G F and Mountford E P 1996 Effects of drought on beech in Lady Park Wood, an unmanaged mixed deciduous woodland *Forestry* **69** 125–36
Phillips N, Bond B J, McDowell N G and Ryan M G 2002 Canopy and hydraulic conductance in young, mature and old Douglas-fir trees *Tree Physiol.* **22** 205–11
Phillips O L *et al* 2009 Drought sensitivity of the amazon rainforest *Science* **323** 1344–7
Phillips O L, Sullivan M J P, Baker T R, Monteagudo Mendoza A, Vargas P N and Vásquez R 2019 Species matter: wood density influences tropical forest biomass at multiple scales *Surv. Geophys.* **40** 913–35
Powell T L *et al* 2013 Confronting model predictions of carbon fluxes with measurements of Amazon forests subjected to experimental drought *New Phytol.* **200** 350–65
Pugh T A M, Lindeskog M, Smith B, Poulter B, Arneth A, Haverd V and Calle L 2019 Role of forest regrowth in global carbon sink dynamics *Proc. Natl Acad. Sci.* **116** 4382–7
Pugh T A M *et al* 2020 Understanding the uncertainty in global forest carbon turnover *Biogeosciences* **17** 3961–89
Quesada C A *et al* 2012 Basin-wide variations in Amazon forest structure and function are mediated by both soils and climate *Biogeosciences* **9** 2203–46
Rodell M *et al* 2004 The global land data assimilation system *Bull. Am. Meteorol. Soc.* **85** 381–94
Rowland L *et al* 2015 Death from drought in tropical forests is triggered by hydraulics not carbon starvation *Nature* **528** 119–22
Saatchi S S *et al* 2011 Benchmark map of forest carbon stocks in tropical regions across three continents *Proc. Natl Acad. Sci.* **108** 9899–904

Sakschewski B et al 2021 Variable tree rooting strategies are key for modelling the distribution, productivity and evapotranspiration of tropical evergreen forests *Biogeosciences* **18** 4091–116

Santiago L S, De Guzman M E, Baraloto C, Vogenberg J E, Brodie M, Hérault B, Fortunel C and Bonal D 2018 Coordination and trade-offs among hydraulic safety, efficiency and drought avoidance traits in Amazonian rainforest canopy tree species *New Phytol.* **218** 1015–24

Saxton K E, Rawls W J, Romberger J S and PAPENDiCK R I 1988 Estimating generalized soil-water characteristics from texture *Soil Sci. Soc. Am. J.* **50** 1031–6

Schnitzer S A and Bongers F 2011 Increasing liana abundance and biomass in tropical forests: emerging patterns and putative mechanisms: increasing lianas in tropical forests *Ecol. Lett.* **14** 397–406

Smith B, Prentice I C and Sykes M T 2001 Representation of vegetation dynamics in the modelling of terrestrial ecosystems: comparing two contrasting approaches within European climate space: vegetation dynamics in ecosystem models *Glob. Ecol. Biogeogr.* **10** 621–37

Smith B, Warlind D, Arneth A, Hickler T, Leadley P, Siltberg J and Zaehle S 2014 Implications of incorporating N cycling and N limitations on primary production in an individual-based dynamic vegetation model *Biogeosciences* **11** 2027–54

Tardieu F and Simonneau T 1998 Variability among species of stomatal control under fluctuating soil water status and evaporative demand: modelling isohydric and anisohydric behaviours *J. Exp. Bot.* **49** 419–32

Tejada G, Görgens E B, Espírito-Santo F D B, Cantinho R Z and Ometto J P 2019 Evaluating spatial coverage of data on the aboveground biomass in undisturbed forests in the Brazilian Amazon *Carbon Balance Manage.* **14** 11

Terrer C *et al* 2021 A trade-off between plant and soil carbon storage under elevated CO_2 *Nature* **591** 599–603

Trenberth K E, Dai A, van der Schrier G, Jones P D, Barichivich J, Briffa K R and Sheffield J 2014 Global warming and changes in drought *Nat. Clim. Change* **4** 17–22

Trugman A T, Detto M, Bartlett M K, Medvigy D, Anderegg W R L, Schwalm C, Schaffer B and Pacala S W 2018 Tree carbon allocation explains forest drought-kill and recovery patterns *Ecol. Lett.* **21** 1552–60

Urli M, Porte A J, Cochard H, Guengant Y, Burlett R and Delzon S 2013 Xylem embolism threshold for catastrophic hydraulic failure in angiosperm trees *Tree Physiol.* **33** 672–83

Weedon G P, Gomes S, Viterbo P, Shuttleworth W J, Blyth E, Österle H, Adam J C, Bellouin N, Boucher O and Best M 2011 Creation of the WATCH forcing data and its use to assess global and regional reference crop evaporation over land during the twentieth century *J. Hydrometeorol.* **12** 823–48

Whitehead D 1998 Regulation of stomatal conductance and transpiration in forest canopies *Tree Physiol.* **18** 633–44

Whitehead D, Edwards W R N and Jarvis P G 1984 Conducting sapwood area, foliage area and permeability in mature trees of Picea sitchensis and Pinus contorta *Can. J. Forest Res.* **14** 940–7

Xu X, Medvigy D, Powers J S, Becknell J M and Guan K 2016 Diversity in plant hydraulic traits explains seasonal and inter-annual variations of vegetation dynamics in seasonally dry tropical forests *New Phytol.* **212** 80–95

Yang J, Tian H, Pan S, Chen G, Zhang B and Dangal S 2018 Amazon drought and forest response: largely reduced forest photosynthesis but slightly increased canopy greenness during the extreme drought of 2015/2016 *Glob. Change Biol.* **24** 1919–34

Yao Y, Ciais P, Viovy N, Joetzjer E and Chave J 2023 How drought events during the last century have impacted biomass carbon in Amazonian rainforests *Glob. Change Biol.* **29** 747–62